Pentacoordinate Nickel(II) Complexes Double Bridged by Phosphate Ester or Phosphinate Ligands: Spectroscopic, Structural, Kinetic, and Magnetic Studies

M. Dolores Santana,*[a] Gabriel García,*[a] A. Abel Lozano,[a] Gregorio López,[a] José Tudela,[b] José Pérez,[c] Luis García,[c] Luis Lezama,[d] and Teófilo Rojo[d]

Abstract: The bis(phosphatediester)-bridged complexes $[\{Ni([12]aneN_3)(\mu\text{-}O_2P(OR)_2)\}_2](PF_6)_2$ {$[12]aneN_3 = Me_3[12]aneN_3$, 2,4,4-trimethyl-1,5,9-triazacyclododec-1-ene; R = Me (**1**), Bu (**2**), Ph (**3**), Ph-4-NO_2 (**4**); $[12]aneN_3 = Me_4[12]aneN_3$, 2,4,4,9-tetramethyl-1,5,9-triazacyclododec-1-ene; R = Me (**5**), Bu (**6**), Ph (**7**), Ph-4-NO_2 (**8**)} were prepared by hydrolysis of the phosphate triester with the hydroxo complex $[\{Ni([12]aneN_3)(\mu\text{-}OH)\}_2](PF_6)_2$ or by acid–base reaction of the dialkyl or diaryl phosphoric acid and the above hydroxo complex. The acid–base reaction was also used to synthesise the phosphinate-bridged complexes $[\{Ni([12]aneN_3)(\mu\text{-}O_2PR_2)\}_2](PF_6)_2$ {$[12]aneN_3 = Me_3[12]aneN_3$, R = Me (**9**), Ph (**10**); $[12]aneN_3 = Me_4[12]aneN_3$, R = Me (**11**), Ph (**12**)}. The molecular structures of complexes **2**, **3** and **12** were established by single crystal X-ray diffraction studies. The eight-membered rings defined by the nickel atoms and the bridging ligands show distorted twist-boat, chair and boat–boat conformations in **2**, **3** and **12**, respectively. The experimental susceptibility data for compounds **2**, **3** and **12** were fitted by least-squares methods to the analytical expression given by Ginsberg. The best fit was obtained with values of $J = -0.11\ cm^{-1}$, $D = -9.5\ cm^{-1}$ and $g = 2.20$ for **2**; $J = -0.97\ cm^{-1}$, $D = -9.3\ cm^{-1}$ and $g = 2.21$ for **3**; and $J = -0.14\ cm^{-1}$, $D = -11.9\ cm^{-1}$ and $g = 2.195$ for **12**. The magnetic-exchange pathways must involve the phosphate/phosphinate bridges, because these favour antiferromagnetic interactions. The observation of a higher exchange parameter for compound **3** is a consequence of a favourable disposition of the O–P–O bridges. The kinetics for the hydrolysis of TNP (tris(4-nitrophenyl)phosphate) with the dinuclear nickel(II) hydroxo complex $[\{Ni(Me_3[12]aneN_3)(\mu\text{-}OH)\}_2](PF_6)_2$ was studied by UV-visible spectroscopy. The proposed mechanism for TNP-promoted hydrolysis can be described as one-substrate/two-product, and can be fitted to a Michaelis–Menten equation.

Keywords: kinetics · magnetic properties · nickel · phosphates · phosphinates

Introduction

Many enzymes, including those that hydrolyse phosphate esters, use two metal ions in a bifunctional catalytic mechanism.[1] For example, phosphotriesterases, which hydrolyse phosphate triesters and have been employed as insecticides and chemical warfare agents, require divalent metal ions (Zn, Cd, Ni, Co, Mn) for their activities.[2] The binuclear Zn^{II} ion site of the phosphotriesterase (PTE) from *Pseudomonas diminuta* has been confirmed by a 2.1 Å resolution X-ray crystal structure.[3] Nonredox-active metal ions such as Ni^{II} and Zn^{II} are potentially of interest as hydrolytic cleaving agents. Moreover, their reactivity in model systems may lead to functional DNA-cleaving molecules, because synthetic metal complexes can be used as simple model systems for hydrolytic enzymes. To this purpose, dinuclear Cu^{II},[4] Co^{III},[5] La^{III}[6] or Zn^{II}[7] complexes have been studied in order to analyse the binding and activation of phosphate

[a] Dr. M. D. Santana, Prof. G. García, A. A. Lozano, Prof. G. López
Departamento de Química Inorgánica
Universidad de Murcia, 30071 Murcia (Spain)
Fax: (+34) 968-364148
E-mail: ggarcia@um.es

[b] Dr. J. Tudela
Departamento de Bioquímica y Biología Molecular A
Universidad de Murcia, 30071 Murcia (Spain)

[c] Dr. J. Pérez, Dr. L. García
Departamento de Ingeniería Minera, Geológica y Cartográfica
Universidad Politécnica de Cartagena
30203 Cartagena (Spain)

[d] Dr. L. Lezama, Prof. T. Rojo
Departamento de Química Inorgánica
Facultad de Ciencias, Universidad del País Vasco
48080 Bilbao (Spain)

Supporting information for this article is available on the WWW under http://www.chemeurj.org/ or from the author.

DOI: 10.1002/chem.200305367

esters. Interestingly, Ni^{II}-substituted phosphotriesterase has a higher specific activity than the native Zn^{II} enzyme.[2] However, synthetic nickel(II) complexes that are able to hydrolyse phosphate esters are rare.[8] Recently, in order to understand the mechanistic roles of the metal ions in phosphate ester hydrolysis, Yamaguchi et al. reported the hydrolysis activities of hydroxo- or carboxylate-bridged dinuclear Ni^{II} and Cu^{II} complexes.[9] They found that the hydrolysis activities of the dinuclear Ni^{II} complexes were significantly higher than those of the Cu^{II} and Zn^{II} complexes. On the other hand, Cheng and co-workers prepared an iron(III)–nickel(II) heterodinuclear complex with a bridging and a terminal diphenylphosphate.[10] Although these nickel(II) complexes contained one bridging phosphate group, dinuclear pentacoordinate nickel(II) complexes bridged solely by two phosphate ester (or phosphinate) ligands have not been reported. Thus, to augment our understanding of hydroxo-bridged dinickel(II) complexes we here describe the syntheses and characterisation of pentacoordinate dinuclear nickel(II) complexes that contain two bridging phosphate ester or phosphinate ligands. Moreover, we investigated the ability of the dinuclear nickel(II) hydroxo complex $[\{Ni(Me_3[12]aneN_3)(\mu\text{-}OH)\}_2](PF_6)_2$ ($Me_3[12]aneN_3$ = 2,4,4-trimethyl-1,5,9-triazacyclododec-1-ene) and its 9-methyl derivative ($Me_4[12]aneN_3$),[11] to promote the hydrolysis of phosphate esters. We also report a study conducted on the geometrical conformation of the bridging unit and its role in the magnetic interactions that arise between the nickel ions.

Results and Discussion

The green bis(phosphate)-bridged dinuclear complexes $[\{Ni([12]aneN_3)(\mu\text{-}O_2P(OR)_2)\}_2](PF_6)_2$ (**1**–**8**) can be prepared in acetone in two different ways (Scheme 1). They can be obtained by hydrolysis of the phosphate triester with the hydroxo complex $[\{Ni([12]aneN_3)(\mu\text{-}OH)\}_2](PF_6)_2$ (Scheme 1a) or by acid–base reaction of the dialkyl or diaryl phosphoric acid and the above hydroxo complex (2:1 molar ratio) (Scheme 1b). The hydrolytic synthesis afforded lower yields of **1**–**8** and required longer reaction times. As described in Scheme 1c, the acid–base reaction provided higher yields (82–93%) and could be applied to the synthesis of the phosphinate-bridged complexes $[\{Ni([12]aneN_3)(\mu\text{-}O_2PR_2)\}_2](PF_6)_2$ (**9**–**12**). These complexes are green or blue-green solids that are stable to air both in the solid state and in solution. The new complexes have been characterised by partial elemental analysis, FAB^+ mass spectrometry and spectroscopic (UV-visible, IR, ^1H NMR) techniques.

The electronic spectra of **1**–**12** are quite similar and show two d–d transitions in acetone with λ_{max} (ε) between 620–640 nm ($\sim 30\,M^{-1}cm^{-1}$) and 380—390 nm ($\sim 100\,M^{-1}cm^{-1}$). These can be assigned to $^3B_1(F)\rightarrow{}^3E(F)$ and $^3B_1(F)\rightarrow{}^3A_2,{}^3E(P)$ transitions, respectively.[12] Both λ_{max} values and molar absorptivities are consistent with a five-coordinate environment around the nickel(II) ion,[13] and provide evidence that the molecule maintains its integrity in solution.

The IR spectra of complexes **1**–**12** show characteristic absorptions for the $[12]aneN_3$ ligands[13]: 3291–3258 cm^{-1} ν(N–H), ~1660 cm^{-1} ν(C=N), and two strong bands as a result of the PF_6^- ion at 840 and 560 cm^{-1}. The IR spectra of **1**–**8** also exhibit two bands in the 1164–1045 and 924–905 cm^{-1} regions; these can be assigned to the ν((P)-O-C) and ν(P-O-(C)) vibrations, respectively.[14] The bands caused by the $\nu_a(PO_2)$ and $\nu_s(PO_2)$ vibrations fall in the 1264–1202 and 1122–976 cm^{-1} regions, respectively, for complexes **1**–**8** and in the 1293–1189 and 1196–1077 cm^{-1} regions for complexes **9**–**12**. The bands around 450 cm^{-1} can be assigned to ν(Ni–O) vibrations.

The ^1H NMR spectra of the complexes exhibit relatively sharp and well-resolved resonances, and have a chemical shift range that spans over 350 ppm. The representative ^1H NMR spectra for complexes **7** and **10** are shown in Figures 1 and 2, respectively. Assignments of the relatively sharp isotropically shifted resonances were made on the basis of our previous experience with similar paramagnetic pentacoordinate nickel(II) complexes.[15] The spectra show the expected resonance line pattern, and because of a dominant spin-polarisation mechanism, the eight resonance signals for the α-CH protons are shifted downfield, whereas the six resonance signals for the β-CH protons are shifted upfield, with respect to the diamagnetic position. Furthermore, axial protons are expected to experience smaller contact shifts than equatorial protons, because of the angular dependence of the hyperfine coupling constant.[16] The spectra of certain derivatives exhibited separate downfield reso-

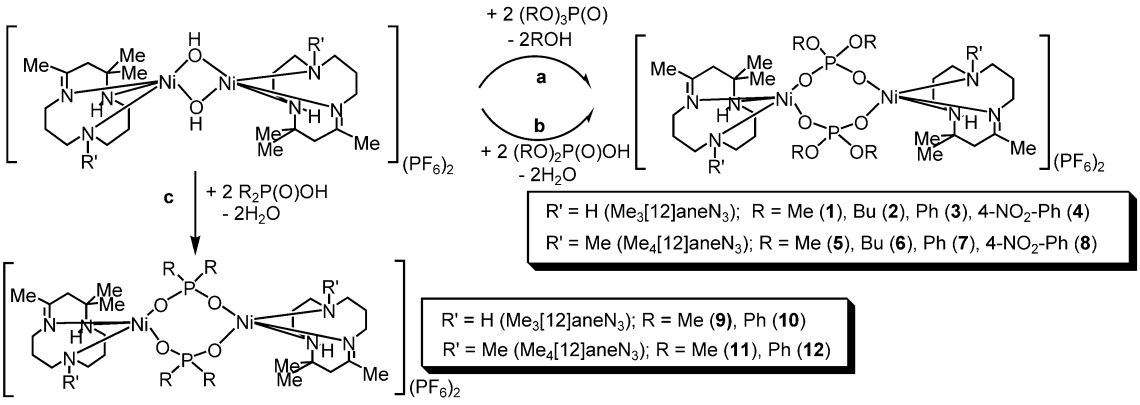

Scheme 1. Scheme showing the different routes to complexes **1**–**12**.

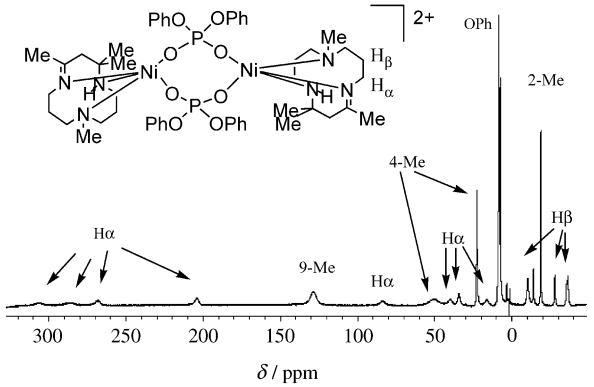

Figure 1. ^{1}H NMR spectra (in [D$_6$]acetone at room temperature) of compound **7**.

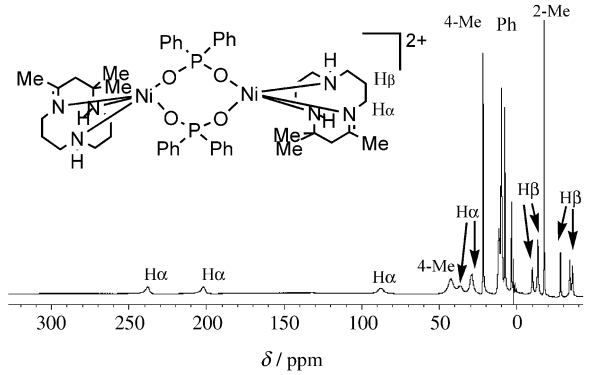

Figure 2. ^{1}H NMR spectra (in [D$_6$]acetone at room temperature) of compound **10**.

nances for the α-protons (Figure 1), whereas in other cases the signals were not well resolved, because of the large line width (Figure 2). Moreover, the isotropically shifted resonance signals observed for the methyl groups appear as follows: 2-Me, ~−17 ppm; 4-Me(a,b), ~40 and 20 ppm; and 9-Me, ~120 ppm.[15] The resonance signals for the alkyl and aryl groups of the phosphate ester and phosphinate ligands farthest from the nickel atom had smaller shifts with respect to the diamagnetic position, and were all downfield from the signal for TMS. This is to be expected in a system that contains a dominant σ-delocalisation pattern of spin density, as well as two unpaired electrons in the ground state nickel(II) σ-symmetry orbitals ($d_{x^2-y^2}$, d_{z^2}). Finally, it is noteworthy that the magnitude of the downfield shifts is greatest for the phosphinate derivatives (6.5 ppm for **1** versus 14.5 ppm for **9**).

Crystal structures: The crystal structures for the cations of complexes **2**, **3** and **12** are shown in Figures 3, 4 and 5, respectively, while selected bond lengths and bond angles are contained in Table 1.

The coordination geometry around the nickel atom is distorted trigonal bipyramidal for **2** and distorted square pyramidal for **3**. This can be ascertained by the Reedijk's τ parameter[17] ($\tau = 0$ and 1 for square-pyramidal and trigonal-bipyramidal structures, repectively), which has a value of 0.4 and 0.0 for complexes **2** and **3**, respectively. In complex **12**,

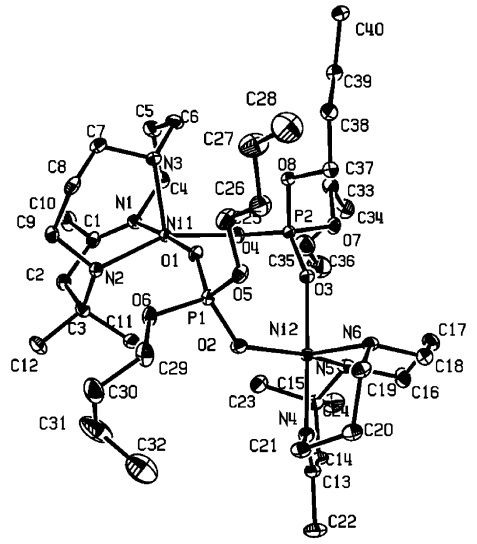

Figure 3. ORTEP plot of the cation of [{Ni(Me$_3$[12]aneN$_3$)(μ-O$_2$P(OBu)$_2$)}$_2$](PF$_6$)$_2$ (**2**).

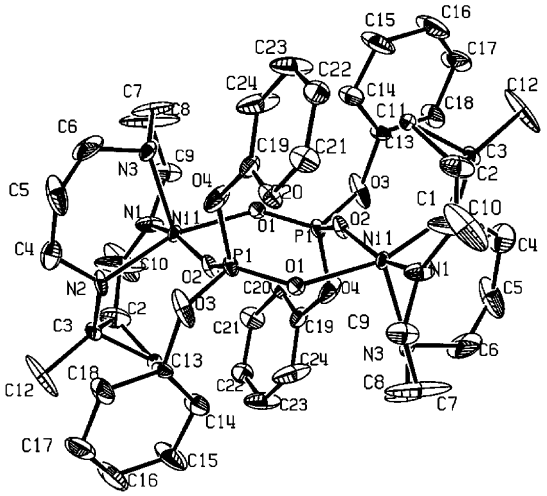

Figure 4. ORTEP plot of the cation of [{Ni(Me$_3$[12]aneN$_3$)(μ-O$_2$P(OPh)$_2$)}$_2$](PF$_6$)$_2$ (**3**).

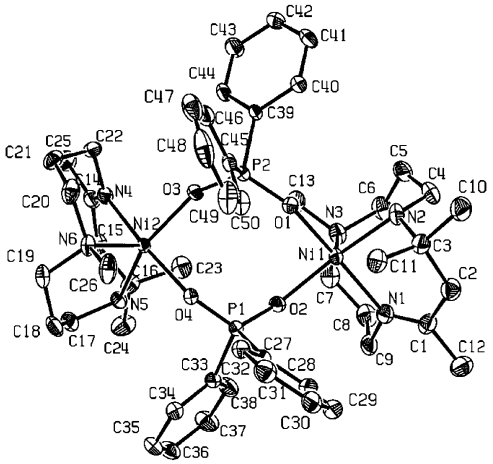

Figure 5. ORTEP plot of the cation of [{Ni(Me$_4$[12]aneN$_3$)(μ-O$_2$PPh$_2$)}$_2$](PF$_6$)$_2$·2 Me$_2$CO·Et$_2$O (**12**).

Table 1. Selected bonds [Å] and angles [°] for **2**, **3** and **12**.

	2	**3**	**12**
Ni1–N1	2.038(3)	2.029(5)	2.053(4)
Ni1–N2	2.056(3)	2.044(5)	2.081(4)
Ni1–N3	2.039(4)	2.031(5)	2.065(5)
Ni1–O1	2.034(3)	2.026(4)	2.025(3)
Ni1–O2	2.010(3)	2.032(4)	2.027(3)
Ni2–N4	2.030(4)	–	2.062(4)
Ni2–N5	2.043(4)	–	2.079(4)
Ni2–N6	2.034(4)	–	2.064(4)
Ni2–O3	2.021(3)	–	1.988(3)
Ni2–O4	2.022(3)	–	2.043(3)
N1–Ni1–N2	90.96(15)	91.9(2)	88.43(17)
N1–Ni1–N3	–	94.8(2)	93.15(18)
N2–Ni1–N3	–	101.4(2)	99.78(17)
N1–Ni1–O1	–	162.56(19)	161.98(16)
N1–Ni1–O2	–	90.6(2)	90.32(15)
N2–Ni1–O1	–	85.87(19)	85.72(15)
N2–Ni1–O2	–	163.82(19)	163.19(15)
N3–Ni1–O1	–	101.4(2)	104.63(16)
N3–Ni1–O2	–	95.61(18)	97.02(16)
O1–Ni1–O2	–	86.96(14)	90.39(13)
N4–Ni2–N5	–	–	88.10(16)
N4–Ni2–N6	–	–	92.37(16)
N5–Ni2–N6	–	–	102.36(16)
N4–Ni2–O3	–	–	88.17(14)
N4–Ni2–O4	–	–	172.64(14)
N5–Ni2–O3	–	–	146.45(15)
N5–Ni2–O4	–	–	90.77(15)
N6–Ni2–O3	–	–	111.10(15)
N6–Ni2–O4	–	–	94.97(14)
O3–Ni2–O4	–	–	88.77(12)

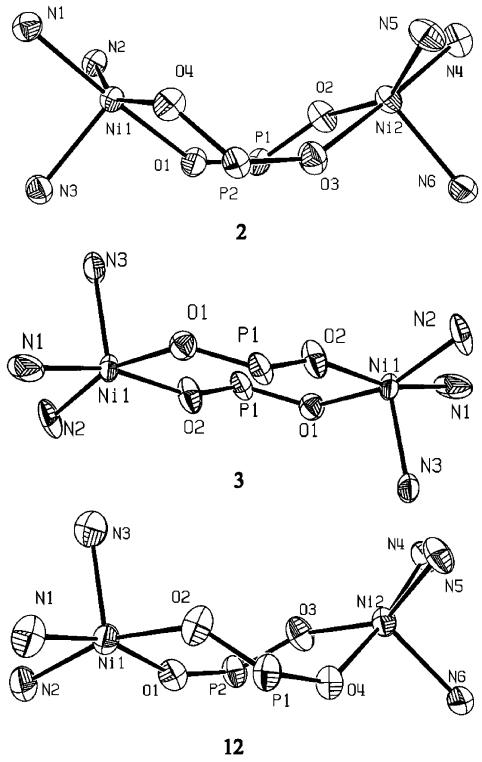

Figure 6. ORTEP view of the eight-membered rings of the bridge core showing the atom-labelling scheme.

the geometry around each nickel atom is very different ($\tau =$ 0.0 and 0.4 for Ni1 and Ni2, respectively).

The coordinated macrocycles in complexes **2** and **12** exhibit chairlike conformations in the two six-membered rings that do not contain the C=N bond. This is the most frequent conformation in complexes that contain such macrocycles.[18]

In accord with the classification from Allen et al.,[19] the eight-membered rings defined by the nickel atoms and the bridging ligands show a distorted twist-boat, chair and boat–boat conformation for complexes **2**, **3** and **12**, respectively (Figure 6). The torsion angles in the complexes do not conform to the ideal of around 20°.

The Ni···Ni distances are 4.863(1), 5.424(1) and 5.116(1) Å for **2**, **3** and **12**, respectively. These distances indicate a flattening of the eight-membered ring that constitutes the bridge core (least-square planes defined by the eight-membered ring have a root mean square (rms) of 0.502, 0.097 and 0.419 for **2**, **3** and **12**, respectively). Moreover, the Ni···Ni distance for **3** is longer than those reported for the $[M_2(\mu\text{-phosphato})_2]$ core (M···M is 4.189 Å when M = Fe,[20] and ranges from 4.931 to 5.367 Å when M = V[21,22]).

Magnetic properties: The thermal variation of the inverse of the magnetic molar susceptibility (χ_m^{-1}) and the $\chi_m T$ product for compounds **2**, **3** and **12** are shown in Figure 7. As can be seen, the Curie–Weiss law is only followed in the high temperature range. Values of $C_m = 2.42$ (**2**), 2.45 (**3**) and 2.41 $cm^3 K mol^{-1}$ (**12**), and $\theta = -0.7$ (**2**), -2.6 (**3**) and -0.8 K (**12**) have been calculated. In each case the $\chi_m T$ product decreases as the temperature decreases, and this occurs more

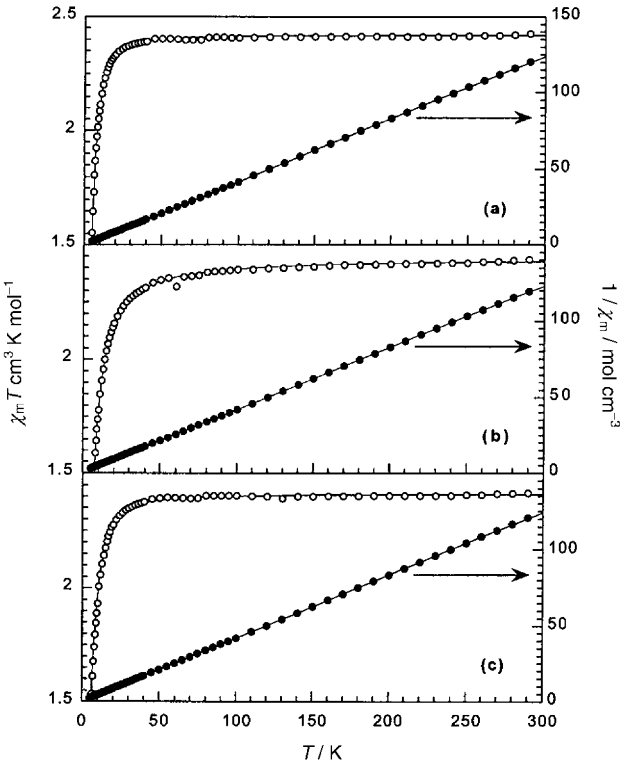

Figure 7. Thermal evolution of χ_m^{-1} and $\chi_m T$ for compounds **2** (a), **3** (b) and **12** (c). Solid lines on the $\chi_m T$ curves correspond to the best fits obtained using the Ginsberg equation. Solid lines on the χ_m^{-1} curves correspond to the expected Curie–Weiss behaviour.

rapidly below 50 K. This behaviour, which is usually associated with a large nickel(II) single-ion zero-field splitting, indicates the existence of a weak antiferromagnetic coupling between the metallic centers.

For the theoretical analysis of the magnetic behaviour of compounds **2**, **3** and **12**, the analytical expression developed by Ginsberg et al.[23] was used. This is based upon the following Hamiltonian in which the nickel(II) ion is assumed to be magnetically isotropic [Eq. (1)]:

$$\mathbf{H} = -2J\mathbf{S_1}\mathbf{S_2} - D(S_{1z^2} + S_{2z^2}) - g\beta H(\mathbf{S_1} + \mathbf{S_2}) - z'J'\mathbf{S}\langle\mathbf{S}\rangle \qquad (1)$$

In Equation (1) J is the usual intradimeric exchange parameter, while D is the zero-field splitting of the single-ion ground state in which a negative value corresponds to the $M_s = 0$ value lying below the $M_1 = \pm 1$ doublet. Because of the possible interdimer contacts, a mean field correction term to the Hamiltonian, which is parameterised by $z'J'$, was also included. It is worth mentioning that the parameters D and $z'J'$ are very strongly correlated to each other, but are only weakly correlated to g and J. As a result, the estimated g and J values are more accurate than the D and $z'J'$ values.

The experimental susceptibility data for compounds **2**, **3** and **12** were least-squares fitted to the analytical expression given by Ginsberg. The best fit was obtained with values of: $J = -0.11\ cm^{-1}$, $D = -9.5\ cm^{-1}$ and $g = 2.20$ (**2**); $J = -0.97\ cm^{-1}$, $D = -9.3\ cm^{-1}$ and $g = 2.21$ (**3**); and $J = -0.14\ cm^{-1}$, $D = -11.9\ cm^{-1}$ and $g = 2.195$ (**12**). Introduction of a reasonable $z'J'$ parameter did not improve the quality of the fit and this term was finally neglected. The excellent agreement between the experimental and calculated data for the three compounds can be observed in Figure 7. The zero-field splitting of octahedral Ni^{II} compounds and the consequences this has on the magnetic properties have been extensively studied.[24] High D values, as large as $20\ cm^{-1}$ in some compounds, are commonly observed in distorted environments.[25] However, calculations for D terms on Ni^{II} pentacoordinate complexes are not available. To support the validity of the D values obtained for compounds **2**, **3** and **12**, EPR measurements were carried out at X band, but no signals were observed in the temperature range 4.2–300 K. These results are in good agreement with the values calculated for the zero-field splitting parameters. In considering the structural features exhibited by these compounds, the magnetic exchange pathways must involve the phosphate/phosphinate bridges (Ni–O–P–O–Ni). From ^{31}P NMR studies it is well known that spin transfer through s and p phosphorous orbitals plays an important role in the exchange mechanisms of many transition-metal phosphates.[26,27] Moreover, these types of exchange pathways usually favour antiferromagnetic interactions. If the angles that correspond to the Ni–O–P–O–Ni exchange pathways (Table 2) and Goodenough's rules[28] are taken into account, the interactions in compounds **2**, **3** and **12** were expected to be antiferromagnetic, and indeed, are in good agreement with the experimental results. The low calculated J values are not surprising if one considers the relatively large distances between paramagnetic centers (See Table 2). The higher exchange parameter observed for compound **3** is a consequence of the favourable disposition of the O–P–O bridges; these are practically coplanar with the $d_{x^2-y^2}$ magnetic orbitals in the Ni^{II} ions (see Figure 6). The coordination geometry around the nickel atoms is square pyramidal for **3**. The basal atoms and the bridging ligands define a least-square plane that has an rms of 0.211, and the Ni atoms are displaced 0.291(2) Å out of the basal plane toward the apical atom. To our knowledge, the present complexes are the first pentacoordinate nickel(II) compounds with this type of bridge. Moreover, in six-coordinated Ni^{II} phosphates/phosphonates, even if this type of bridge is not unusual, the exchange interactions are mainly propagated through oxygen atoms shared by two adjacent polyhedra. Therefore, a comparative analysis of the sign and strength of the magnetic interactions cannot be carried out. However, it is noteworthy that the study performed by Gao et al. on a family of Ni^{II} diphosphonates, in which nickel(II) is simultaneously six-, five- and fourfold coordinate, indicates the existence of very weak exchange interactions that have magnetic orderings below 4 K.[29]

Table 2. Selected distances and angles for Ni-O-P-O-Ni magnetic-exchange pathways for complexes **2**, **3** and **12** (atom labels are given in Figure 6).

	Interacting atoms	Ni–Ni[a] [Å]	Ni-O-P [°]	P-O-Ni [°]
2	Ni1-O1-P1-O2-Ni2	7.028(3)	146.7(2)	132.6(2)
	Ni1-O4-P2-O3-Ni2	7.018(3)	128.2(19)	151.3(2)
3	Ni1-O1-P1-O2-Ni2	7.014(4)	136.5(2)	157.2(3)
12	Ni1-O1-P2-O3-Ni2	7.022(3)	154.7(2)	148.9(2)
	Ni1-O2-P1-O4-Ni2	7.073(3)138.6(2)	139.5(2)	

[a] Length of exchange pathway.

Kinetics of the tris(4-nitrophenyl)phosphate hydrolysis: We examined the hydrolysis of TNP (tris(4-nitrophenyl)phosphate) with the dinuclear nickel(II) hydroxo complex [{Ni(Me_3[12]aneN_3)(μ-OH)}$_2$](PF_6)$_2$ (L1Ni–OH) as a model reaction for PTE by UV-visible spectroscopy. The proposed mechanism for TNP hydrolysis by the dinuclear metal complex can be described as one-substrate/two-product (Scheme 2); this is analogous to the enzymatic catalysis of

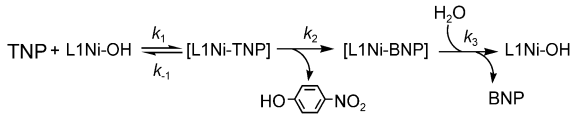

Scheme 2. One-substrate/two-product mechanism for TNP hydrolysis in the presence of a dinuclear Ni^{II} complex.

PTE proposed recently.[30] The steady-state rate of 4-nitrophenol (4NP) formation (V_o) should display an hyperbolic dependence with TNP and must be able to be fitted to a Michaelis–Menten equation [Eq. (2)]:

$$V_0 = \frac{V_{max}[TNP]_0}{K_M + [TNP]_0} = \frac{k_{cat}[L1Ni{-}OH]_0[TNP]_0}{K_M + [TNP]_0} \qquad (2)$$

in which $k_{cat}=k_2k_3/(k_2+k_3)$ and $K_M=k_3(k_{-1}+k_2)/k_1(k_2+k_3)$. The proposed molecular mechanism is depicted in Scheme 3. In this mechanism, TNP binds to the nickel(II)

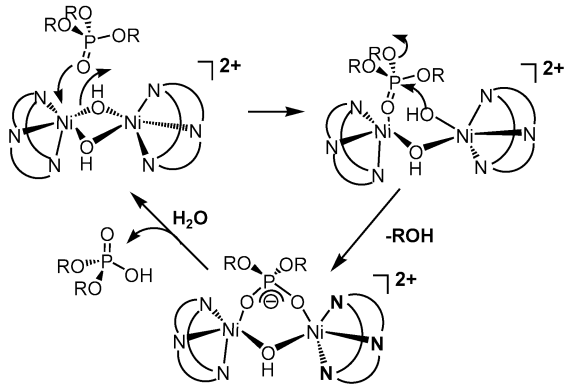

Scheme 3. Proposed molecular mechanism for the hydrolysis of phosphate triesters in the presence of a dinuclear Ni^{II} complex.

atom by coordinating to the phosphoryl oxygen. This interaction then weakens the binding of the bridging hydroxide to the second nickel(II) atom. The metal–oxygen interaction polarises the phosphoryl–oxygen bond and makes the phosphorous atom more electrophilic. As a consequence of the nucleophilic attack by the bound hydroxide, the bond to the leaving group weakens. In the next step, a molecule of 4NP is released and a dinuclear nickel(II) complex in which a phosphate diester bridges the nickel atoms is obtained. Finally, the diester phosphate is displaced by a water molecule to regenerate the catalyst. This mechanism is supported by the crystal structure of the nickel(II) complex which has two bridging phosphodiesters and was prepared by triester phosphate hydrolysis.

The solubilities of TNP and (L1Ni–OH) were tested in several organic solvents. The best results were obtained with acetone and MeCN. A kinetic study was carried out in which the linearity of the time-drive recordings, the negligible TNP hydrolysis in the absence of catalyst, as well as the concentration effects of H_2O, L1Ni–OH and TNP were taken into consideration (Supporting Information). The kinetic behaviour followed the Michaelis–Menten model [Eq. (2)]. Plots of the hydrolysis rate (V_0) against $[TNP]_0$ gave a saturation curve (Figure 8). In accordance with the reaction mechanism proposed, this fact suggests the reversible formation of a (L1Ni-TNP) complex prior to TNP hydrolysis. Thus, the Michaelis–Menten equation was applied, and the catalytic (k_{cat}) and Michaelis constant (K_M) were determined by nonlinear regression fittings (Table 3).

Only a few kinetic studies on the hydrolysis of phosphotriesters have been undertaken, and most of them have been conducted in aqueous media. Kady et al.[31] found that mononuclear Zn^{II} models with N_3 and N_3O ligands showed k_{obs} values of between 4.5×10^{-2} and $1.5\times10^{-6}\,s^{-1}$ for diethyl(4-nitrophenyl)phosphate hydrolysis in water. Itoh et al.[32] studied the catalytic hydrolysis of 2,4-dinitrophenyl ethylphosphate using mononuclear Cu^{II} complexes with N_3 ligands. These displayed k_{cat} values of between 0.7×10^{-6} and

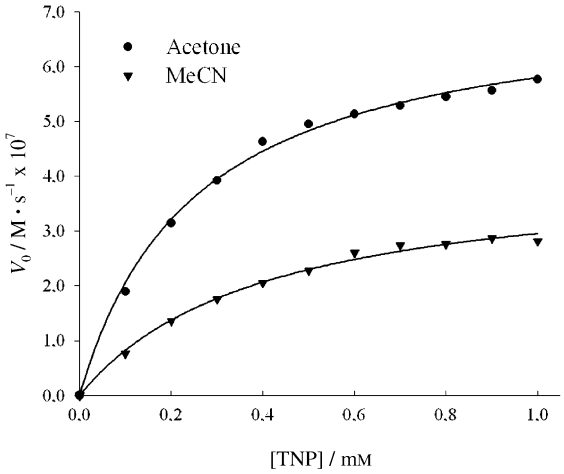

Figure 8. Michaelis–Menten kinetics for the hydrolysis of TNP with L1Ni–OH. Acetone (●), MeCN (▼), and nonlinear regression fitted to Equation (2) (——). Assay conditions: 2.5% H_2O, $[L1Ni–OH]=10\,\mu M$, 20 °C.

Table 3. Kinetic parameters[a] for L1Ni–OH hydrolysis of TNP.

Solvent	k_{cat} [$s^{-1}\times10^2$]	K_M [mM]	k_{cat}/K_M [$M^{-1}s^{-1}$]
acetone	7.3 ± 0.1	0.25 ± 0.01	292 ± 12
MeCN	4.1 ± 0.1	0.40 ± 0.03	103 ± 8

[a] Assay conditions: 2.5% H_2O, $[L1Ni–OH]=10\,\mu M$, 20 °C. Nonlinear regression fitted to Equation (2), $R^2>0.99$.

$1.6\times10^{-3}\,s^{-1}$. If the different reaction media are not considered, then the kinetic parameters for the [{Ni(Me_3[12]-aneN_3)(μ-OH)}$_2$](PF_6)$_2$ hydrolysis of TNP are an improvement on the previously published results for other models, but are still a far cry from the kinetic parameters obtained for the paraoxon hydrolysis of PTE[30] ($k_{cat}=3000\,s^{-1}$ and $k_{cat}/K_M=5\cdot10^7\,M^{-1}s^{-1}$).

Experimental Section

General methods: C, H and N analyses were carried out with a microanalyser Carlo Erba model EA 1108. Infrared spectra were recorded on a Perkin–Elmer 16F PC FT-IR spectrophotometer on Nujol mulls between polyethylene sheets. The UV-visible spectra (in acetone) were recorded over the 300–800 nm range on a UNICAM 520 spectrophotometer equipped with matched quartz cells. The ^1H NMR spectra were recorded on a Bruker model AC 200E or a Bruker AV-400 spectrometer. Fast-atom bombardment (FAB) mass spectra were run on a Fisons VG Autospec spectrometer operating in the FAB^+ mode. Magnetic susceptibilities of powdered samples were measured in the 5–300 K temperature range with a Quantum Design MPMS-7 SQUID magnetometer. The experimental susceptibilities were corrected for the diamagnetism of the sample holders and the constituent atoms (Pascal tables), as well as for temperature-independent paramagnetism (estimated to be $100\times10^{-6}\,cm^3mol^{-1}$). A Bruker ESP300 spectrometer operating at X band and equipped with standard Oxford low-temperature devices was used to record the ESR powder spectra at different temperatures. The magnetic field was calibrated by an NMR probe and the frequency inside the cavities was determined with a Hewlett–Packard 5352B microwave frequency counter. Most chemicals were purchased from Aldrich and were used without further purification. Tris(4-nitrophenyl)phosphate (TNP) was obtained from Fluka, whereas acetone and acetonitrile (MeCN) of chromatographic quality (<0.1% water) were purchased from Merck. Milli-Q system (Mil-

lipore Corp.) ultrapure water was used. Solvents were dried and distilled by general methods before use. The complexes $[\{Ni(Me_3[12]aneN_3)(\mu\text{-}OH)\}_2](PF_6)_2$ ($Me_3[12]aneN_3$ = 2,4,4-trimethyl-1,5,9-triazacyclododec-1-ene) and its 9-methyl derivative ($Me_4[12]aneN_3$) were prepared by previously described procedures.[11]

$[\{Ni([12]aneN_3)(\mu\text{-}O_2P(OR)_2)\}_2](PF_6)_2$ {$[12]aneN_3 = Me_3[12]aneN_3$, R = Me (1), Bu (2), Ph (3), Ph-4-NO_2 (4); $[12]aneN_3 = Me_4[12]aneN_3$, R = Me (5), Bu (6), Ph (7), Ph-4-NO_2 (8)}: Complexes **1–8** were prepared by reaction of $[\{Ni([12]aneN_3)(\mu\text{-}OH)\}_2](PF_6)_2$ (0.12 mmol) with the corresponding tris(alkyl) or tris(aryl) phosphate (0.24 mmol) in acetone (25 mL). After stirring for 24 h the solution was concentrated under reduced pressure, and upon addition of diethyl ether a green solid precipitated. This was collected by filtration, washed with diethyl ether and air-dried. Yields: 57–78%. Higher yields of **1–8** were obtained from a mixture of $[\{Ni([12]aneN_3)(\mu\text{-}OH)\}_2](PF_6)_2$ (0.12 mmol) and dialkyl or diaryl phosphoric acid (0.24 mmol) in acetone (25 mL). After stirring for 3 h the solutions were handled in a manner analogous to that described above. Yields: 82–93%.

Compound 1: ^{1}H NMR ([D$_6$]acetone, TMS): δ = 236.1 (H$_\alpha$), 234.3 (H$_\alpha$), 201.6 (H$_\alpha$), 89.5 (H$_\alpha$), 48.2 (3H; 4-Me), 33.8 (H$_\alpha$), 32.4 (H$_\alpha$), 28.7 (H$_\alpha$), 21.8 (3H; 4-Me), 16.5 (H$_\alpha$), 6.5 (3H; OMe), −9.7 (H$_\beta$), −13.1 (2H; H$_\beta$), −16.9 (3H; 2-Me), −27.8 (H$_\beta$), −33.1 (H$_\beta$), −34.6 ppm (H$_\beta$); IR (nujol): $\tilde{\nu}$ = 3286, 3259 (N−H), 1662 (C=N), 1242 (PO_2)$_a$, 1045 ((P)-O-C), 981 (PO_2)$_s$, 908 (P-O-(C)), 469 cm^{-1} (Ni−O); MS (FAB$^+$): *m/z* (%): 394 (100) $[M/2]^+$; elemental analysis calcd (%): for $C_{28}H_{62}F_{12}N_6Ni_2O_8P_4$ (1080.1): C 31.14, H 5.79, N 7.78; found: C 31.05, H 6.10, N 7.71.

Compound 2: ^{1}H NMR ([D$_6$]acetone, TMS): δ = 235.9 (H$_\alpha$), 234.0 (H$_\alpha$), 202.4 (H$_\alpha$), 89.4 (H$_\alpha$), 49.1 (3H; 4-Me), 34.5 (H$_\alpha$), 32.9 (H$_\alpha$), 28.7 (H$_\alpha$), 21.9 (3H; 4-Me), 17.1 (H$_\alpha$), 7.9 (2H; OCH_2), 4.4 (2H; CH_2), 3.2 (2H; CH_2), 1.3 (3H; CH_3), −9.9 (H$_\beta$), −13.3 (2H; H$_\beta$), −17.2 (3H; 2-Me), −27.9 (H$_\beta$), −33.6 (H$_\beta$), −35.1 ppm (H$_\beta$); IR (nujol): $\tilde{\nu}$ = 3286, 3258 (N−H), 1660 (C=N), 1245 (PO_2)$_a$, 1065 ((P)-O-C), 976 (PO_2)$_s$, 905 (P-O-(C)), 468 cm^{-1} (Ni−O); MS (FAB$^+$): *m/z* (%): 1101 (4) $[M]^+$, 478 (100) $[M/2]^+$; elemental analysis calcd (%) for $C_{40}H_{86}F_{12}N_6Ni_2O_8P_4$ (1248.4): C 38.48, H 6.94, N 6.73; found: C 38.36, H 6.75, N 6.91.

Compound 3: ^{1}H NMR ([D$_6$]acetone, TMS): δ = 250.0 (H$_\alpha$), 219.5 (H$_\alpha$), 89.2 (2H; H$_\alpha$), 53.5 (3H; 4-Me), 37.1 (H$_\alpha$), 36.7 (H$_\alpha$), 32.9 (H$_\alpha$), 22.4 (3H; 4-Me), 17.5 (H$_\alpha$), 7.9 (3H; OPh), 7.3 (2H; OPh), −10.1 (H$_\beta$), −13.8 (2H; H$_\beta$), −18.3 (3H; 2-Me), −28.3 (H$_\beta$), −34.8 (H$_\beta$), −36.1 ppm (H$_\beta$); IR (nujol): $\tilde{\nu}$ = 3278, 3260 (N−H), 1658 (C=N), 1202 (PO_2)$_a$, 1102 ((P)-O-C), 1024 (PO_2)$_s$, 910 (P-O-(C)), 444 cm^{-1} (Ni−O); MS (FAB$^+$): *m/z* (%): 1181 (5) $[M]^+$, 518 (100) $[M/2]^+$; elemental analysis calcd (%) for $C_{48}H_{70}F_{12}N_6Ni_2O_8P_4$ (1328.4): C 43.40, H 5.31, N 6.33; found: C 43.45, H 5.53, N 6.30.

Compound 4: ^{1}H NMR ([D$_6$]acetone, TMS): δ = 251.6 (H$_\alpha$), 232.6 (H$_\alpha$), 91.4 (2H; H$_\alpha$), 56.8 (3H; 4-Me), 40.3 (H$_\alpha$), 34.5 (2H; H$_\alpha$), 22.4 (3H; 4-Me), 18,3 (H$_\alpha$), 8.6 (2H; OPh-4-NO_2), 7.3 (2H; OPh-4-NO_2), −9.7 (H$_\beta$), −13.5 (2H; H$_\beta$), −17.1 (3H; 2-Me), −28.5 (H$_\beta$), −34.7 (H$_\beta$), −35.9 ppm (H$_\beta$); IR (nujol): $\tilde{\nu}$ = 3266 (N−H), 1662 (C=N), 1213 (PO_2)$_a$, 1161 ((P)-O-C), 1098 (PO_2)$_s$, 910 (P-O-(C)), 452 cm^{-1} (Ni−O); MS (FAB$^+$): *m/z* (%): 1361 (4) $[M]^+$, 608 (22) $[M/2]^+$; elemental analysis calcd (%) for $C_{48}H_{66}F_{12}N_{10}Ni_2O_{16}P_4$ (1508.4): C 38.22, H 4.41, N 9.29; found: C 37.97, H 4.63, N 9.21.

Compound 5: ^{1}H NMR ([D$_6$]acetone, TMS): δ = 292.5 (H$_\alpha$), 267.0 (H$_\alpha$), 250.3 (H$_\alpha$), 186.0 (H$_\alpha$), 118.2 (3H; 9-Me), 83.9 (H$_\alpha$), 46.4 (3H; 4-Me), 41.4 (H$_\alpha$), 32.7 (H$_\alpha$), 22,5 (3H; 4-Me), 16.1 (H$_\alpha$), 6.9 (3H; OMe), −9.5 (2H, H$_\beta$), −12.7 (H$_\beta$), −17.4 (3H; 2-Me), −27.4 (H$_\beta$), −33.4 (H$_\beta$), −34.7 ppm (H$_\beta$); IR (nujol): $\tilde{\nu}$ = 3267 (N−H), 1658 (C=N), 1264 (PO_2)$_a$, 1107 ((P)-O-C), 1058 (PO_2)$_s$, 909 (P-O-(C)), 466 cm^{-1} (Ni−O); MS (FAB$^+$): *m/z* (%): 961 (5) $[M]^+$, 408 (100) $[M/2]^+$; elemental analysis calcd (%) for $C_{30}H_{66}F_{12}N_6Ni_2O_8P_4$ (1108.1): C 32.52, H 6.00, N 7.58; found: C 32.36, H 6.10, N 7.53.

Compound 6: ^{1}H NMR ([D$_6$]acetone, TMS): δ = 292.4 (H$_\alpha$), 271.1 (H$_\alpha$), 248.6 (H$_\alpha$), 184.3 (H$_\alpha$), 118.2 (3H; 9-Me), 84.9 (H$_\alpha$), 45.5 (3H; 4-Me), 33.9 (H$_\alpha$), 31.8 (H$_\alpha$), 22.5 (3H; 4-Me), 14.1 (H$_\alpha$), 8.5 (2H; OCH_2), 3.5 (2H; CH_2), 3.1 (2H; CH_2), 1.5 (3H; CH_3), −9.3 (H$_\beta$), −10.0 (H$_\beta$), −12.5 (H$_\beta$), −17.4 (3H; 2-Me), −27.6 (H$_\beta$), −34.0 (H$_\beta$), −34.8 ppm (H$_\beta$); IR (nujol): $\tilde{\nu}$ = 3264 (N−H), 1658 (C=N), 1230 (PO_2)$_a$, 1100 ((P)-O-C), 1028 (PO_2)$_s$, 909 (P-O-(C)), 462 cm^{-1} (Ni−O); MS (FAB$^+$): *m/z* (%): 1130 (3) $[M]^+$, 492 (100) $[M/2]^+$; elemental analysis calcd (%) for $C_{42}H_{90}F_{12}N_6Ni_2O_8P_4$ (1276.5): C 39.52, H 7.11, N 6.58; found: C 39.35, H 7.31, N 6.54.

Compound 7: ^{1}H NMR ([D$_6$]acetone, TMS): δ = 303.1 (H$_\alpha$), 282.9 (H$_\alpha$), 265.6 (H$_\alpha$), 202.0 (H$_\alpha$), 127.8 (3H; 9-Me), 83.2 (H$_\alpha$), 50.0 (3H; 4-Me), 40.0 (H$_\alpha$), 34.2 (H$_\alpha$), 22.5 (3H; 4-Me), 16.3 (H$_\alpha$), 8.3 (3H; OPh), 7.5 (2H; OPh), −10.1 (2H; H$_\beta$), −13.8 (H$_\beta$), −18.5 (3H; 2-Me), −27.4 (H$_\beta$), −35.1 (H$_\beta$), −35.8 ppm (H$_\beta$); IR (nujol): $\tilde{\nu}$ = 3262 (N−H), 1660 (C=N), 1204 (PO_2)$_a$, 1164 ((P)-O-C), 1122 (PO_2)$_s$, 924 (P-O-(C)), 480 cm^{-1} (Ni−O); MS (FAB$^+$): *m/z* (%): 1209 (12) $[M]^+$, 532 (100) $[M/2]^+$; elemental analysis calcd (%) for $C_{50}H_{74}F_{12}N_6Ni_2O_8P_4$ (1356.4): C 44.27, H 5.50, N 6.20; found: C 44.34, H 5.68, N 6.01.

Compound 8: ^{1}H NMR ([D$_6$]acetone, TMS): δ = 314.2 (H$_\alpha$), 285.7 (H$_\alpha$), 271.6 (H$_\alpha$), 215.7 (H$_\alpha$), 131.4 (3H; 9-Me), 82.3 (H$_\alpha$), 55.8 (3H; 4-Me), 40.7 (H$_\alpha$), 36.1 (H$_\alpha$), 23.2 (3H; 4-Me), 15.1 (H$_\alpha$), 8.7 (2H; OPh-4-NO_2), 7.5 (2H; OPh-4-NO_2), −9.7 (2H; H$_\beta$), −13.6 (H$_\beta$), −18.2 (3H; 2-Me), −27.6 (H$_\beta$), −36.0 ppm (2H; H$_\beta$); IR (nujol): $\tilde{\nu}$ = 3267 (N−H), 1661 (C=N), 1213 (PO_2)$_a$, 1161 ((P)-O-C), 1102 (PO_2)$_s$, 906 (P-O-(C)), 449 cm^{-1} (Ni−O); MS (FAB$^+$): *m/z* (%): 1388 (4) $[M]^+$, 622 (100) $[M/2]^+$; elemental analysis calcd (%) for $C_{50}H_{70}F_{12}N_{10}Ni_2O_{16}P_4$ (1536.4): C 39.09, H 4.59, N 9.12; found: C 39.03, H 4.86, N 8.97.

$[\{Ni([12]aneN_3)(\mu\text{-}O_2PR_2)\}_2](PF_6)_2$ {$[12]aneN_3 = Me_3[12]aneN_3$, R = Me (9), Ph (10); $[12]aneN_3 = Me_4[12]aneN_3$, R = Me (11), Ph (12)}: Complexes **9–12** were prepared by allowing $[\{Ni([12]aneN_3)(\mu\text{-}OH)\}_2](PF_6)_2$ (0.12 mmol) to react with the corresponding alkyl or aryl phosphinic acid (0.24 mmol) in acetone (25 mL). After stirring for 30 min, the solvent was removed under reduced pressured and diethyl ether was added to the solution. This was then cooled to −18 °C, and the resultant blue-green solid was collected by filtration, washed with diethyl ether and air-dried.

Compound 9: Yield: 0.110 g (97%); ^{1}H NMR ([D$_6$]acetone, TMS): δ = 236.4 (H$_\alpha$),185.0 (H$_\alpha$), 86.5 (H$_\alpha$), 42.1 (3H; 4-Me), 36.2 (H$_\alpha$), 30.5 (H$_\alpha$), 28.5 (H$_\alpha$), 27.1 (H$_\alpha$), 21.6 (3H; 4-Me), 19.0 (H$_\alpha$), 14.5 (3H; Me), −8.9 (H$_\beta$), −13.1 (2H; H$_\beta$), −17.0 (3H; 2-Me), −27.5 (H$_\beta$), −32.9 (H$_\beta$), −34.1 ppm (H$_\beta$); IR (nujol): $\tilde{\nu}$ = 3291, 3266 (N−H), 1660 (C=N), 1293 (PO_2)$_a$, 1196 (PO_2)$_s$, 1065 (P−C), 449 cm^{-1} (Ni−O); MS (FAB$^+$): *m/z* (%): 869 (7) $[M]^+$, 362 (100) $[M/2]^+$; elemental analysis calcd (%) for $C_{28}H_{62}F_{12}N_6Ni_2O_4P_4$ (1016.1): C 33.10, H 6.15, N 8.27; found: C 33.09, H 6.23, N 8.21.

Compound 10: Yield: 0.133 g (95%); ^{1}H NMR ([D$_6$]acetone, TMS): δ = 237.8 (2H; H$_\alpha$), 202.0 (H$_\alpha$), 87.9 (H$_\alpha$), 42.6 (3H; 4-Me), 36.6 (2H; H$_\alpha$), 29.0 (2H; H$_\alpha$), 21.7 (3H; 4-Me), 11.5 (2H; Ph), 10.0 (2H; Ph), 7.7 (1H; Ph), −10.1 (H$_\beta$), −13.5 (2H; H$_\beta$), −17.5 (3H; 2-Me), −28.2 (H$_\beta$), −34.2 (H$_\beta$), −35.8 ppm (H$_\beta$); IR (nujol): $\tilde{\nu}$ = 3272 (N−H), 1657 (C=N), 1189 (PO_2)$_a$, 1130 (PO_2)$_s$, 1044 (P−C), 456 cm^{-1} (Ni−O); MS (FAB$^+$): *m/z* (%): 1118 (6) $[M]^+$, 486 (100) $[M/2]^+$; elemental analysis calcd (%) for $C_{48}H_{70}F_{12}N_6Ni_2O_4P_4$ (1264.4): C 45.60, H 5.58, N 6.65; found: C 45.42, H 5.60, N 6.61.

Compound 11: Yield: 0.096 g (82%); ^{1}H NMR ([D$_6$]acetone, TMS): δ = 271.6 (2H; H$_\alpha$), 259.5 (H$_\alpha$), 168.7 (H$_\alpha$), 109.8 (3H; 9-Me), 80.3 (H$_\alpha$), 37.3 (3H; 4-Me), 28.9 (2H; H$_\alpha$), 21.6 (3H; 4-Me), 18.5 (H$_\alpha$), 12.8 (3H; Me), −8.7 (H$_\beta$), −11.5 (H$_\beta$), −13.0 (H$_\beta$), −17.4 (3H; 2-Me), −26.4 (H$_\beta$), −31.9 (H$_\beta$), −33.7 ppm (H$_\beta$); IR (nujol): $\tilde{\nu}$ = 3269 (N−H), 1658 (C=N), 1203 (PO_2)$_a$, 1077 (PO_2)$_s$, 1026 (P−C), 435 cm^{-1} (Ni−O); MS (FAB$^+$): *m/z* (%): 897 (6) $[M]^+$, 376 (100) $[M/2]^+$; elemental analysis calcd (%) for $C_{30}H_{66}F_{12}N_6Ni_2O_4P_4$ (1044.1): C 34.51, H 6.37, N 8.05; found: C 34.39, H 6.34, N 7.99.

Compound 12: Yield: 0.132 g (91%); ^{1}H NMR ([D$_6$]acetone, TMS): δ = 285.8 (H$_\alpha$), 254.6 (H$_\alpha$), 246.5 (H$_\alpha$), 185.3 (H$_\alpha$), 118.2 (3H; 9-Me), 86.0 (2H; H$_\alpha$), 36.7 (3H; 4-Me), 28.7 (2H; H$_\alpha$), 20.4 (3H; 4-Me), 12.7 (2H; Ph), 10.5 (2H; Ph), 8.3 (1H; Ph), −9.8 (H$_\beta$), −11.8 (H$_\beta$), −12.9 (H$_\beta$), −17.6 (3H; 2-Me), −27.7 (H$_\beta$), −33.5 (H$_\beta$), −35.0 ppm (H$_\beta$); IR (nujol): $\tilde{\nu}$ = 3266 (N−H), 1658 (C=N), 1194 (PO_2)$_a$, 1128 (PO_2)$_s$, 1045 (P−C), 456 cm^{-1} (Ni−O); MS (FAB$^+$): *m/z* (%): 1146 (5) $[M]^+$, 500 (100) $[M/2]^+$; elemental analysis calcd (%) for $C_{50}H_{74}F_{12}N_6Ni_2O_4P_4 \cdot 2Me_2CO \cdot Et_2O$ (1482.7): C 48.60, H 6.52, N 5.67; found: C 48.45, H 6.46, N 5.81.

Determination of the X-ray crystal structure of compounds 2, 3 and 12: Crystals of $[\{Ni(Me_3[12]aneN_3)(\mu\text{-}O_2P(OBu)_2)\}_2](PF_6)_2$ (**2**), $[\{Ni(Me_3[12]aneN_3)(\mu\text{-}O_2P(OPh)_2)\}_2](PF_6)_2$ (**3**) and $[\{Ni(Me_4[12]aneN_3)(\mu\text{-}O_2PPh_2)\}_2](PF_6)_2 \cdot 2Me_2CO \cdot Et_2O$ (**12**) suitable for X-ray diffraction studies were grown from acetone/diethyl ether liquid diffusion. In all cases, crystals

Table 4. Crystal data and structure refinement for **2**, **3** and **12**.

	2	**3**	**12**
formula	$C_{40}H_{86}F_{12}N_6Ni_2O_8P_4$	$C_{48}H_{70}F_{12}N_6Ni_2O_8P_4$	$C_{50}H_{74}F_{12}N_6Ni_2O_4P_4{\cdot}2\,Me_2CO{\cdot}Et_2O$
M_r	1248.45	1328.40	1482.73
crystal system	monoclinic	triclinic	triclinic
a [Å]	12.0309(9)	10.1955(9)	12.5277(16)
b [Å]	20.3278(12)	11.1727(9)	13.0101(12)
c [Å]	12.6585(11)	13.1453(11)	24.744(2)
α [°]	90	99.699(6)	99.698(7)
β [°]	111.285(6)	96.955(6)	96.253(9)
γ [°]	90	104.977(5)	116.679(9)
V [Å^3]	2884.6(4)	1404.4(2)	3473.2(6)
T [K]	173(2)	173(2) K	173(2)
space group	$P2(1)$	$P1$	$P1$
Z	2	1	2
λ [Å]	0.71073	0.71073	0.71073
μ [mm^{-1}]	0.852	0.881	0.719
reflections collected	10630	7782	12686
independent reflections	10152 ($R_{int}=0.0172$)	4902 ($R_{int}=0.0259$)	12082 ($R_{int}=0.0281$)
goodness of fit on F^2	1.033	1.053	0.873
final R indices $[I>2\sigma(I)]$[a,b]	$R_1=0.0454$, $wR_2=0.1200$	$R_1=0.0642$, $wR_2=0.1732$	$R_1=0.0560$, $wR_2=0.1369$
R indices (all data)[a,b]	$R_1=0.0515$, $wR_2=0.1242$	$R_1=0.0869$, $wR_2=0.1857$	$R_1=0.1022$, $wR_2=0.1528$
max/min $\Delta\rho$ [e Å^{-3}]	1.074/−0.495	0.666/−0.608	0.681/−0.607

[a] $R_1=\Sigma\,\|\,F_o|-|F_c\|/\Sigma|F_o|$ for reflections with $I>2\sigma I$. [b] $wR_2=\{\Sigma[w(F_o^2-F_c^2)^2]/\Sigma[w(F_o^2)^2]\}^{1/2}$ for all reflections; $w^{-1}=\sigma^2(F^2)+(aP)^2+bP$, in which $P=(2F_c^2+F_o^2)/3$ and a and b are constants set by the program.

were mounted on glass fibres and transferred to a Siemens P4 diffractometer. The crystallographic data are summarised in Table 4. Cell constants were refined from 65 (**2**), 57 (**3**) or 64 (**12**) reflections in the 2θ range 10–25°. The structures were solved by the heavy-atom method and refined anisotropically.[33] Hydrogen atoms were included using a riding model. For compound **3**, the macrocycle that involves N1 and N3, a phenyl group and the $(PF_6)^-$ ion are disordered over two positions.

CCDC-215907 (**2**), CCDC-215908 (**3**) and CCDC-215909 (**12**) contain the supplementary crystallographic data for this paper. These data can be obtained free of charge via www.ccdc.cam.ac.uk/conts/retrieving.html (or from the Cambridge Crystallographic Data Centre, 12 Union Road, Cambridge CB2 1EZ, UK; fax: (+44) 1223-336-033; or deposit@ccdc.cam.uk).

Kinetic analysis: In order to define the best assay conditions, UV-visible spectra of the species implied in the hydrolytic process were recorded ($325<\lambda<400$) in several organic solvents (acetone, MeCN, ethanol and methanol) with different water content (0–12.5%). The hydrolysis rates were measured by the initial slope method following an increase in the absorption band of the hydrolysis product 4-nitrophenol (4NP) in acetone or MeCN solutions as promoted by the metal complex (L1Ni−OH). A typical reaction procedure involved immediate monitoring of the increase in absorbance at 340 nm (owing to the release of 4-nitrophenol) after rapid injection of 100 μL of a 0.3 mM solution of (L1Ni−OH) in acetone (or MeCN) into 2.9 mL of a TNP solution (0.1–1 mM and 2.5% of water) to give a final volume of 3 mL. The concentration range of the substrate was selected around $K_M/5$ to $5{\cdot}K_M$ to improve the reliability of the statistical analysis.[34] Control experiments were made up similarly, but without the presence of the nickel complex. Hydrolysis of bis(4-nitrophenyl)phosphate (BNP) was too slow to be detected under the same conditions. In each kinetic trial, points were recorded every 120 s (8 points s^{-1}). The kinetic data were analysed using the Sigma Plot 4.0 program for WINDOWS™, and were fitted to the Michaelis–Menten equation.[35] At least three independent measurements were made to determine the rate constants.

Acknowledgements

We thank the Fundación Séneca, CARM (Projects PI-32/00800/FS/01 and PI-79/00810/FS/01) for financial support and the Dirección General de Investigación del Ministerio de Ciencia y Tecnología for partial financial support (Project BQU2001–0979-C02). A.A.L. thanks Fundación Seneca for an FPI-grant.

[1] a) E. Kimura, *Prog. Inorg. Chem.* **1994**, *41*, 443–491; b) W. N. Lipscomb, N. Sträter, *Chem. Rev.* **1996**, *96*, 2375–2434; c) D. E. Wilcox, *Chem. Rev.* **1996**, *96*, 2435–2458; d) E. Kimura, T. Koike, *Adv. Inorg. Chem.* **1997**, *44*, 229–261.

[2] G. A. Omburo, J. M. Kuo, L. S. Mullins, F. M. Raushel, *J. Biol. Chem.* **1992**, *267*, 13278–13283.

[3] J. L. Vanhooke, M. M. Benning, F. M. Raushel, H. M. Holden, *Biochemistry* **1996**, *35*, 6020–6025.

[4] a) M. Wall, R. C. Hynes, J. Chin, *Angew. Chem.* **1993**, *105*, 1696–1697; *Angew. Chem. Int. Ed. Engl.* **1993**, *32*, 1633–1634; b) E. Kövári, R. Krämer, *J. Am. Chem. Soc.* **1996**, *118*, 12704–12709; c) J. Gao, A. E. Martell, J. Reibenspies, *Inorg. Chim. Acta*, **2002**, *329*, 122–128.

[5] a) D. H. Vance, A. W. Crzarik, *J. Am. Chem. Soc.*, **1993**, *115*, 12165–12166; b) D. Wahnon, A.-M. Lebuis, J. Chin, *Angew. Chem.* **1995**, *107*, 2594–2597; *Angew. Chem. Int. Ed. Engl.* **1995**, *34*, 2412–2414; c) N. H. Williams, W. Cheung, J. Chin, *J. Am. Chem. Soc.* **1998**, *120*, 8079–8087.

[6] a) B. K. Takasaki, J. Chin, *J. Am. Chem. Soc.* **1993**, *115*, 9337–9338; b) B. K. Takasaki, J. Chin, *J. Am. Chem. Soc.* **1995**, *117*, 8582–8585.

[7] a) T. Koike, M. Inoue, E. Kimura, M. Shiro, *J. Am. Chem. Soc.* **1996**, *118*, 3091–3099; b) C. Bazzicalupi, A. Bencini, A. Bianchi, V. Fusi, C. Giorgi. P. Paoletti, B. Valtancoli, D. Zanchi, *Inorg. Chem.* **1997**, *36*, 2784–2790; c) C. Bazzicalupi, A. Bencini, E. Berni, A. Bianchi, V. Fedi, V. Fusi, C. Giorgi. P. Paoletti, B. Valtancoli, *Inorg. Chem.* **1999**, *38*, 4115–4122; d) P. Jurek, A. E. Martell, *Inorg. Chim. Acta* **1999**, *287*, 47–51; e) D. Kong, A. E. Martell, J. Reibenspies, *Inorg. Chim. Acta* **2002**, *333*, 7–14.

[8] a) M. A. De Rosch, W. C. Trogler, *Inorg. Chem.* **1990**, *29*, 2409–2416; b) J. R. Morrow, L. A. Buttrey, K. A. Berback, *Inorg. Chem.* **1992**, *31*, 16–20.

[9] K. Yamaguchi, F. Akagi, S. Fujinami, M. Suzuki, M. Shionoya, S. Suzuki, *Chem. Commun.* **2001**, 375–376.

[10] L.-H. Yin, P. Cheng, S.-P. Yan, X.-Q. Fu, J. Li, D.-Z. Liao, Z.-H. Jiang, *J. Chem. Soc. Dalton Trans.* **2001**, 1398–1400.

[11] a) J. W. L. Martin, J. H. Johnston, N. F. Curtis, *J. Chem. Soc. Dalton Trans.* **1978**, 68–76; b) A. Escuer, R. Vicente, J. Ribas, *Polyhedron* **1992**, *11*, 453–456.

[12] A. B. P. Lever, *Inorganic Electronic Spectroscopy*, Elsevier, Amsterdam, **1984**, pp. 513–520.
[13] M. D. Santana, G. García, J. Pérez, E. Molins, G. López, *Inorg. Chem.* **2001**, *40*, 5701–5703.
[14] a) P. N. Turowski, W. H. Armstrong, S. Liu, S. N. Brown, S. J. Lippard, *Inorg. Chem.* **1994**, *33*, 636–645; b) H. Adams, N. A. Bailey, D. E. Fenton, Q.-Y. He, *J. Chem. Soc. Dalton Trans.* **1997**, 1533–1539.
[15] a) M. D. Santana, G. García, A. Rufete, G. Sánchez, M. C. Ramírez de Arellano, G. López, *Inorg. Chem. Commun.* **1998**, *1*, 267–269; b) M. D. Santana, G. García, A. Rufete, M. C. Ramírez de Arellano, G. López, *J. Chem. Soc. Dalton Trans.* **2000**, 619–625; c) M. D. Santana, G. García, C. M. Navarro, A. A. Lozano, J. Pérez, L. García, G. López, *Polyhedron* **2002**, *21*, 1935–1942.
[16] a) R. H. Holm and C. J. Hawkins in *NMR of Paramagnetic Molecules*, (Eds.: G. N. La Mar, W. Horrocks, Jr., R. H. Holm) Academic Press, New York, **1973**, p. 243–332; b) A. Dei, M. Wicholas, *Inorg. Chim. Acta* **1989**, *166*, 151–154.
[17] A. W. Addison, T. N. Rao, J. Reedijk, J. V. Rijn, G. C. Verschoor, *J. Chem. Soc. Dalton Trans.* **1984**, 1349–1356.
[18] J. Pérez, L. García, A. G. Orpen, M. D. Santana, P. Saez, G. García, *New J. Chem.* **2002**, *26*, 726–731.
[19] F. H. Allen, J. A. K. Howard, N. A. Pitchford, *Acta Crystallogr. Sect. B* **1996**, *52*, 882–891.
[20] S. Yan, X. Pan, L. F. Taylor, J. H. Zhang, C. J. O'Connor, D. Britton, O. P. Anderson, L. Que Jr. , *Inorg. Chim. Acta* **1996**, *243*, 1–8.
[21] M. R. Bond, L. M. Mokry, T. Otieno, J. Thompson, C. J. Carrano, *Inorg. Chem.* **1995**, *34*, 1894–1905.
[22] N. S. Dean, L. M. Mokry, M. R. Bond, C .J. O'Connor, C. J. Carrano, *Inorg. Chem.* **1996**, *35*, 2818–2825.
[23] A. P. Ginsberg, R. L. Martin, R. W. Brookes, R. C. Sherwood, *Inorg. Chem.* **1972**, *11*, 2884–2889.
[24] R. L. Carlin, *Magnetochemistry*, Springer, Berlin, **1986**.
[25] F. W. Klaaijsen, Z. Dokoupil, W. J. Huiskamp, *Phys. B* **1975**, *79*, 547–567.
[26] L. Lezama, K. S. Suh, G. Villeneuve, T. Rojo, *Solid State Commun.* **1990**, *76*, 449–452.
[27] G. Villeneuve, K. S. Suh, P. Amorós, N. Casan-Pastor, D. Beltrán-Porter, *Chem. Mater.* **1992**, *4*, 108–111.
[28] J. B. Goodenough in: *Magnetism and the Chemical Bond*, Interscience, New York, **1963**.
[29] Q. Gao, N. Guillou, M. Nogues, A. K. Cheetham, G. Férey, *Chem. Mater.* **1999**, *11*, 2937–2947.
[30] F. M. Raushel, *Curr. Opin. Microbiol.* **2002**, *5*, 288–295.
[31] I. O. Kady, B. Tan, Z. Ho, T. Scarborough, *J. Chem. Soc. Chem. Commun.* **1995**, *118*, 1137–1138.
[32] T. Itoh, H. Hisada, Y. Usui, Y. Fujii, *Inorg. Chim. Acta* **1998**, *283*, 51–60.
[33] G. M. Sheldrick, SHELX-97, Programs for Crystal Structure Analysis (Release 97–2), University of Göttingen, Germany, **1998**.
[34] R. D. Allison, D. C. Purich, *Meth. Enzymol.* **1980**, *63*, 3–22.
[35] L. Endrenyi, *Kinetic Data Analysis: Design and Analysis of Enzyme and Pharmacokinetics Experiments*, Plenum Press, New York, **1981**.

Received: July 23, 2003
Revised: October 13, 2003 [F5367]